2007 IEEE International Conference on
Robotics and Automation
Roma, Italy, 10-14 April 2007

Output Feedback Control of Wind Display in a Virtual Environment

Sandip D. Kulkarni, Mark A. Minor, Mark W. Deaver, Eric R. Pardyjak

Abstract—**This research focuses on development of a haptic system to create controlled air flow acting on a user in the Treadport virtual environment. The Treadport Active Wind Tunnel (TPAWT) is thus created in order to produce air flow patterns that allow a variety of wind angles and speeds to be felt by the user. In order to control this system in real-time, the small gain theorem is used in conjunction with a dynamic extension to formulate an output feedback control law. Examples of controller formulations are derived and discrete time simulations in FLUENT demonstrate their effectiveness. The controller is then validated experimentally using a scale model of the TPAWT.**

[1] ***Index Terms*— Virtual Reality, Haptic Interfaces, Flow Control, Input-output stability.**

I. Introduction

ACTIVE flow control has several applications such as reducing flow transients, controlling the instabilities associated with cavity flows, controlling airfoil flow separation, and drag reduction for increased aircraft fuel economy. In this paper, a novel application of active flow control in a virtual environment is presented. Virtual environments mimic the real world, and the goal of virtual reality research is to bring the virtual environment close to the real world ambience. The Treadport virtual reality system, Fig. 1, allows the user to walk through a virtual environment while viewing realistic renderings on a 180° CAVE-like display located at the front and sides of the Treadport [1]. Combinations of Treadport tilt and a tether exerting force on the user render locomotion forces [2]. To create a more realistic sense of immersion for the user, a sense of wind, radiant heat, and olfactory display is thought to be essential.

The primary focus of this research is the real-time control of the wind felt by the user in what we have termed the Treadport Active Wind Tunnel (TPAWT). The TPAWT augments the original treadport with added floor, ceiling, and sidewalls to guide airflow supplied through controllable vents. Air flowing out of the vents is regulated and deflected along the side and front displays in order to be guided toward the user [3], Fig. 2.

As part of this work, a strategy is developed to achieve active control of the wind by creating stable flow patterns. For mathematical simplicity, a planar two-dimensional model of the TPAWT is considered, Fig. 2. The inputs to the TPAWT are the wind speed provided by the left and right vents. The full scale system will have top and bottom vents on

Fig. 1. Sarcos Treadport Locomotion Interface.

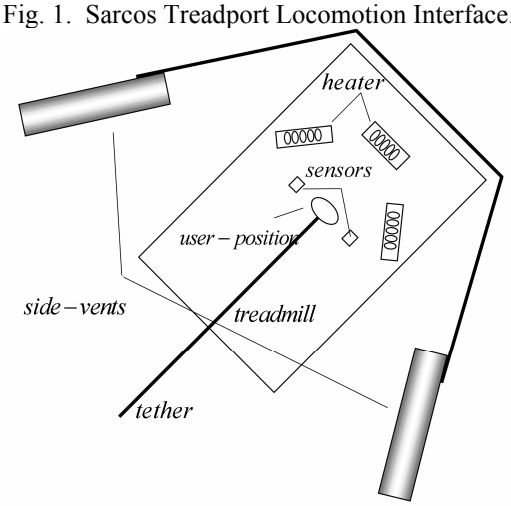

Fig. 2. Plan view of the Treadport Active Wind Tunnel (TPAWT).

Note: This work was supported in part by the National Science Foundation under Grant No. 428856.

S.D. Kulkarni is with the Department of Mechanical Engineering, University of Utah, Salt Lake City, Utah, 84112, USA.

M.A. Minor is with the Department of Mechanical Engineering, University of Utah, Salt Lake City, Utah, 84112, USA (phone: 801-587-7771; fax: 801-585-9826; minor@mech.utah.edu).

M.W. Deaver is with the Department of Mechanical Engineering, University of Utah, Salt Lake City, Utah, 84112, USA.

E.R. Pardyjak is with the Department of Mechanical Engineering, University of Utah, Salt Lake City, Utah, 84112, USA.

each side such that more complex flow patterns can be created. In the planar model, the output of the system is the mean wind velocity at the user position. The outputs of the physical system are provided by sensors in close proximity to the user.

Given that the airflow in the TPAWT can be approximated as a distributed parameter system with an infinite number of degrees of freedom (DOF), we are ultimately controlling the input-output map of an underactuated system. Our approach is based upon linear output-feedback control with a dynamic extension that links spatial sensitivity analysis and temporal response. FLUENT Computational Fluid Dynamics (CFD) analysis is used to provide velocity fields for multiple input velocity conditions. As the simulations show, the direction of flow at the user is linearly dependent upon the ratio of the inlet vent velocities. Magnitude of flow velocity at the user is likewise linearly dependent upon inlet velocities. These linear relationships are the basis of CFD derived geometric Jacobians that are used to formulate the controllers. A dynamic extension and a version of the Small Gain Theorem (SGT) are then used to prove finite-gain *L*-stability of the system while minimizing settling time. This method is computationally effective and well suited for real-time control, which is a notable contribution relative to ongoing active flow control research. Actively controlled wind as provided by the TPAWT can also facilitate alternate applications such as a controllable wind tunnel for evaluating complex fluid structure interaction or for evaluating plume tracking algorithms; to name a few.

The paper is organized as follows. Sect. II compares this research to prior work. Mathematical preliminaries are given in Sect. III and the Input-Output flow is characterized in Sect. IV. The feedback controller is developed in Sect V, and the controller is evaluated in Sect. VI where future work is also discussed. Sect. VII concludes the paper.

II. Background

Distributed parameter models approximate physical phenomena described by continuous partial differential equations as a discrete number of lumped parameter ordinary differential equations. The conventional approach for control of distributed parameter systems is based on spatial discretization. Finite-difference and finite element methods then form systems of ordinary differential equations that serve as a basis for controller design [4-6]. Moreover, controllability, observability, and stability characteristics depend on sensor and actuator locations, discretization method, and a sufficient number of discretization points [7].

Active flow control refers to the manipulation of the system to achieve desired results such as a change in drag or flow separation. Several researchers have structured fluid-flow models to fit within traditional controllers (linear [8, 9], optimal [8, 10, 11], and nonlinear [12, 13]), but there are so many DOF that they are not tractable for real-time control. Thus, control of fluid flow has been studied using reduced order modeling techniques such as Proper Orthogonal Decomposition (POD) [14, 15], Approximate Inertial Manifolds (AIM) [16], and Eigenmode [17] analysis. Model decomposition methods reduce the DOF to a certain extent, but there still remains a vast gap between the DOF required for real-time active-control of wind flow and the DOF after model decomposition. Moreover change in basis with varying flow patterns must be accounted for.

From an alternate perspective, in [18] a LQR controller for thermal processes is developed using distributed parameter control theory and state feedback. This leads to finite dimensional sub-optimal linear output feedback controllers that are similar to our own. Given the complexity of fluid flow models and the requirement for achieving stable flow patterns, this approach is not readily feasible. Rather, the strategy proposed here numerically characterizes the flow at a nominal operating point and designs linear output feedback algorithms based upon the SGT.

The SGT gives a sufficient condition for robust stability of a feedback system so long as the product of the norms of the feedback and plant gains is less than unity. Implementation of the SGT using alternative linear matrix inequality conditions has been applied previously [19, 20] to general multi-dimensional state-space systems. In contrast, we apply the SGT for input-output control of an infinite dimensional system using simple analysis tools.

As far as we know, our application of dynamic extension and the small gain theorem to active flow control is the first such application. Since the method uses an input-output map while considering the system as a black-box, it by-passes the problem of access to the model and is readily applicable to real-time control of a wide range of distributed parameter systems. This paper avoids theoretical aspects of fluid flow control that have limited its practical real-time application.

III. Mathematical Preliminaries

A. Input-Output Map:

Consider the input-output relationship,

$$y = H(u), \tag{1}$$

where H is a mapping operator that specifies y in terms of u. Since systems with unstable parts are to be considered, H cannot be defined as a mapping from L^m to L^q where m and q represent the dimensional spaces of u and y, respectively. An input $u \in L^m$ may generate an output y that does not belong to L^q. Thus, H is defined as a mapping from an extended space $L_e^m = \{u \mid u_\tau \in L^m, \forall\, \tau \in [0,\infty)\}$ to an extended space L_e^q, where u_τ is a truncation of u defined by,

$$u_\tau(t) = \begin{cases} u(t), & 0 \le t \le \tau \\ 0, & t > 0 \end{cases}. \tag{2}$$

Output y is obtained from velocity components measured

by sensors mimicked by the nodes of a line in FLUENT, geometry located close to the user. The input *u* describes the incremented spatial wind velocity provided by the vents.

B. Input-Output Stability [21]:

A mapping $H_1 : L_e^m \to L_e^q$ is *L* stable if there exists a class K function α, defined on [0, ∞), and a non-negative constant β such that

$$\left\|(Hu)_\tau\right\|_L \le \alpha(\left\|u_\tau\right\|_L) + \beta\,, \tag{3}$$

for all $u_\tau \in L^m$ and $\tau \in [0,\infty)$. If it is finite-gain *L* stable, there exist non-negative constants γ and β such that $\left\|(Hu)_\tau\right\|_L \le \gamma(\left\|u_\tau\right\|_L) + \beta$ for all $u \in L^m$ and $\tau \in [0,\infty)$, where β is a bias term that avoids *Hu* from being zero.

C. Small Gain Theorem

Consider the two systems $H_1 : L_e^m \to L_e^q$ and $H_2 : L_e^m \to L_e^q$ shown in Figure 3. Suppose both systems are finite gain *L* stable such that,

$$\begin{aligned} \left\|y_{1\tau}\right\|_L &\le \gamma_1 \left\|e_{1\tau}\right\|_L + \beta_1, \forall e_1 \in L_e^m, \forall \tau \in [0,\infty) \\ \left\|y_{2\tau}\right\|_L &\le \gamma_2 \left\|e_{2\tau}\right\|_L + \beta_2, \forall e_2 \in L_e^q, \forall \tau \in [0,\infty) \end{aligned}, \tag{4}$$

By the Small Gain Theorem, the interconnected feedback system is finite gain *L* stable if [21],

$$\gamma_1\gamma_2 < 1. \tag{5}$$

IV. Input-Output Flow Characterization

Steady flow FLUENT CFD simulations are used for characterizing the flow patterns. Stable vortices are created by the airflow discharged by the vents into the Treadport, Fig. 4. Air flow travels along the screens, collides, and then deflecting back towards the user such that a pair of counter rotating vortices are generated. A stable column of air flow then travels between the vortices, which is naturally aimed towards the user. This allows the user to sense air coming towards them as though it is originating from the scenery displayed on the screens. By controlling the magnitude of the air discharged from the left and right vents, it is possible to control both speed and direction of the wind at the user's position [22].

Stream function plots generated by FLUENT are shown in Fig. 4 that indicate the ability to vary wind direction at the user position. If left and right vent velocities, v_L and v_R, respectively, are equal then the vortices are symmetric and the wind angle is $\theta = 0°$, Fig. 4 (a). If the velocity ratio is $v_L / v_R = 0.76$, then the vortices shift to the left such that a

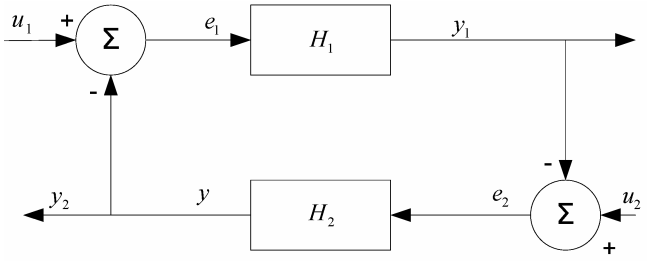

Fig. 3. Interconnected feedback system diagram for Small Gain Theorem.

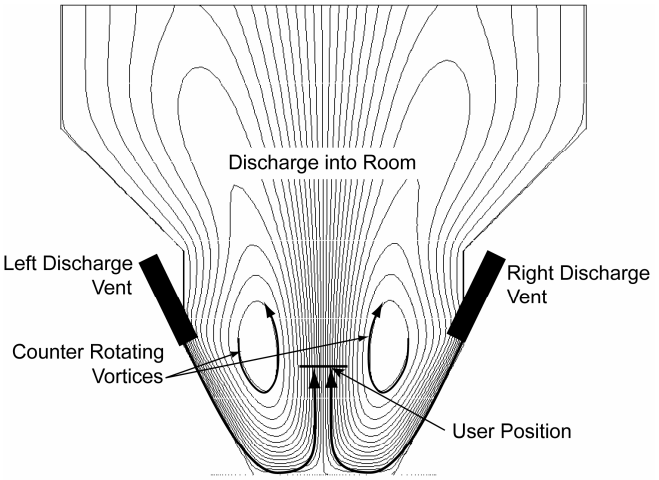

(a) v_L/v_R= 1.00, θ=0 deg

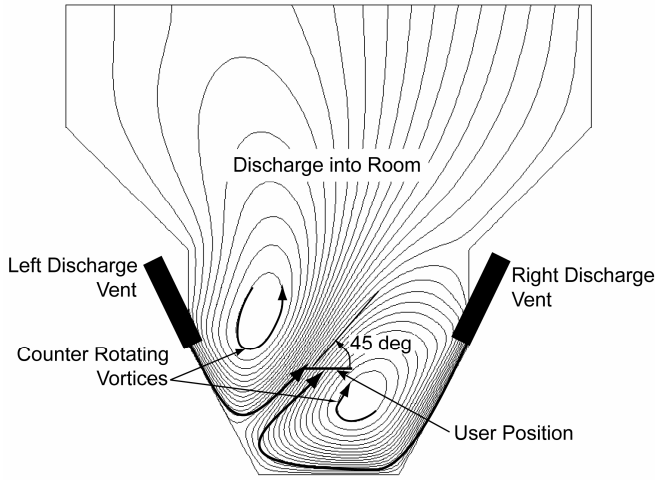

(b) v_L/v_R= 0.76, θ=45 deg

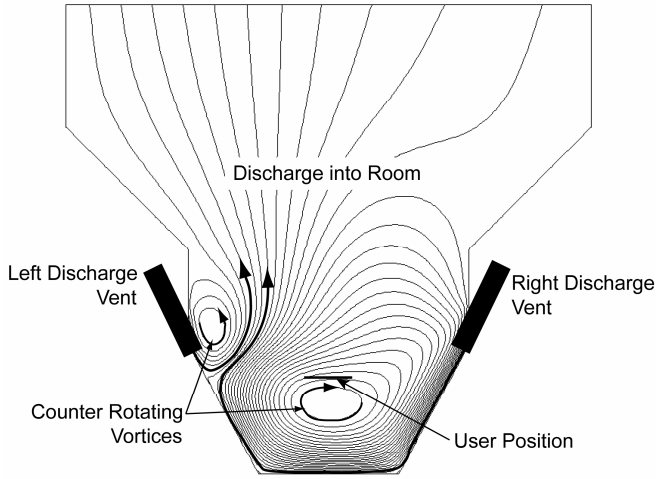

(c) v_L/v_R= 0.50, θ=90 deg

Fig. 4. Stream function plots for varying vent velocity ratios.

wind with a $45°$ heading is created, Fig. 4 (b). If the velocity ratio is decreased further to $v_L / v_R = 0.50$, then the vortices are shifted even further to the left and the wind acting on the person is due to a vortex directly between them and the screen, Fig. 4 (c). In this case, the wind is moving across the person with a heading of $85°$.

The general trend for flow direction as a function of vent velocity ratio was analyzed. A series of simulations were conducted where the ratio was varied for $v_L / v_R = 0.50 \rightarrow 1.50$, Fig. 5. As these results indicate, the wind angle at the user varies over $\theta = 85° \rightarrow -70°$ with respect to vent angle. Asymmetry of this range is due to the increased air pressure at $v_L / v_R = 1.50$, which limits how far the vortices are shifted and thus the range of wind angle at high wind speeds. The Least Squares Fit of this data indicates a linear trend and thus at this stage a desired wind angle is selected by setting the appropriate v_L / v_R ratio from this regression.

Wind speed at a given heading angle was also determined to be linearly proportional to vent outlet velocities. Two test cases were studied for $\theta = 0°$ and $\theta = 45°$ where velocity ratios were $v_L / v_R = 1.00$ and $v_L / v_R = 0.76$, respectively. As Fig. 6 and Fig. 7 indicate, the input-output velocity relationship is fairly linear. These relationships serve as a basis for the following controller implementation.

V. Controller Formulation

A. Construction of the Jacobian matrix:

As the aforementioned results indicate, the input-output relationship of the system is quite linear for a given constant vent velocity ratio. Thus, a truncated Taylor series expansion of the output relative to a nominal input, u_0,

$$y(u) \approx y(u_0) + \left.\frac{\partial y}{\partial u}\right|_{u_0} (u - u_0), \tag{6}$$

provides a linear approximation that defines the geometric Jacobian at u_0 as,

$$J(u_0) = \left.\frac{\partial y}{\partial u}\right|_{u_0} \approx \left.\frac{\delta y}{\delta u}\right|_{u_0}. \tag{7}$$

From (6) we can evaluate the output change, δy, given an input change, δu, as,

$$\delta y = y(u_0 + \delta u) - y(u_0) = J \delta u. \tag{8}$$

Using the results from Fig. 6 and Fig. 7, linear least square estimation is performed to estimate the geometric Jacobian, J, for each vent velocity ratio. The slope of this line is essentially, the Jacobian. The Jacobian for all of the points is obtained by taking a generalized inverse of the input, as

$$J = \Delta y \Delta u^{-1}. \tag{9}$$

B. Dynamic Extension

The error states are defined as $e=y-y_R$ where y_R is the desired output (desired wind speed) and y is the actual output wind speed at the user. Taking the time derivative we have,

$$\dot{e} = \frac{\partial e}{\partial t} = \frac{\partial y}{\partial t} - \frac{\partial y_R}{\partial t}. \tag{10}$$

Applying the chain rule to (10),

$$\dot{e} = \frac{\partial y}{\partial u}\frac{\partial u}{\partial t} - \frac{\partial y_R}{\partial t}, \tag{11}$$

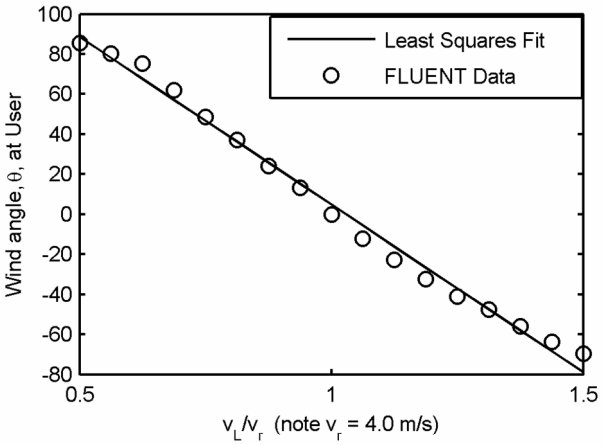

Fig. 5. Wind heading variations as a function of v_L / v_R.

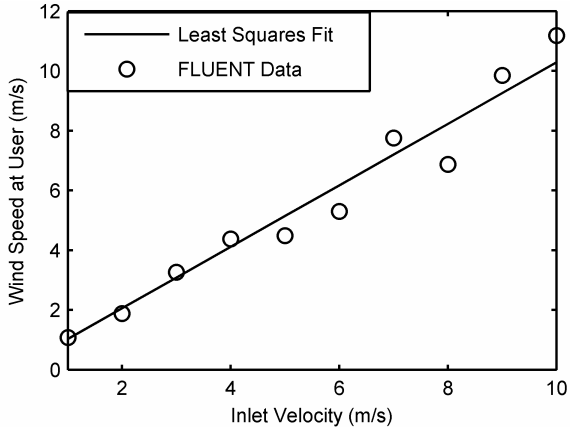

Fig. 6: Wind speed at user given $v_L / v_R = 1.00$ as vent velocity is increased.

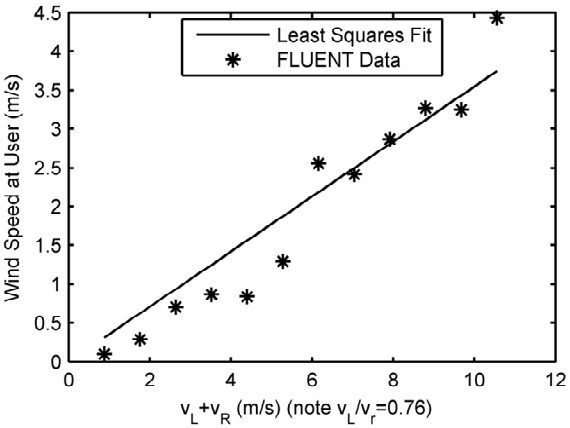

Fig. 7. Wind speed at user given $v_L / v_R = 0.76$ as vent velocity is increased.

and substituting the geometric Jacobian, $J=\frac{\partial y}{\partial u}$, we then have,

$$\dot{e} = J\dot{u} - \frac{\partial y_R}{\partial t} = g(e) . \quad (12)$$

Assigning $g(e) = -Ke$, where $K=K^T>0$ is Hurwitz, we can then solve for the desired control inputs,

$$\dot{u} = J^{-1}\left[Ke + \dot{y}_r\right],$$

in a fashion similar to backstepping. Assuming regulation only, the resulting control system is then expressed as,

$$\begin{aligned} \dot{e} &= -Ke = K\left(y - y_r\right) \\ \dot{u} &= J^{-1}Ke \end{aligned} . \quad (13)$$

Note that the control command u now appears as a state variable. We have applied a dynamic extension to the input. This allows an increase in the relative degree of the system and it ultimately couples the geometric Jacobian indicating spatial sensitivity of the mapping H to be coupled with desired time response as determined explicitly by the gain K. Unique to this controller is that only the Jacobian J is required for a given operating point. This simplicity allows easy implementation of this controller in real-time and requires minimal memory.

C. Applying the Small Gain Theorem

The feedback system (13) can be represented in the form of the simplified interconnected system as shown in Fig. 8. This input-output system is similar to the feedback connection in Fig. 3, analyzed by the small gain theorem. As Fig. 8 indicates, the mapping H_1 is replaced by $J^{-1}K\Delta t$ and H_2 is replaced by J to evaluate stability of the controller. Considering (4) and Fig. 8, we have,

$$\left\|\Delta u\right\| \le \gamma_1 \left\|e\right\|_L + \beta_1 \quad (14)$$

$$\left\|y\right\| \le \gamma_2 \left\|\Delta u\right\|_L + \beta_2 . \quad (15)$$

where $\dot{u}$ is approximated as $\dot{u} \approx \Delta u / \Delta t$ in lieu of a discrete implementation. Thus, the change in control input is $\Delta u_k = \Delta t \cdot J^{-1} \cdot Ke_k$ and the resulting output of the system is $y_{k+1} = Ju_k$. Comparing (14) and (15) with (4), it can be seen that Δu_k and y_{k+1} are analogous to the outputs $y_{1\tau}$ and $y_{2\tau}$. Similarly, e_k in (14) and Δu_k in (15) are like $e_{1\tau}$ and $e_{2\tau}$ in

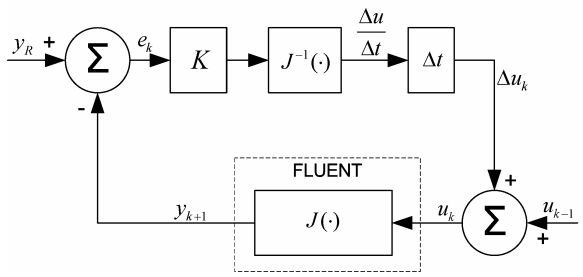

Fig. 8. Equivalent diagram of Small Gain Theorem (SGT) showing discrete controller implementation.

(4), respectively. Taking norms we get,

$$\left\|\Delta u\right\|_L \le \Delta t \left\|J^{-1}K\right\|_L \left\|e\right\|_L \le \Delta t \left\|J^{-1}\right\|_L \left\|K\right\|_L \left\|e\right\|_L \quad (16)$$

$$\text{and } \left\|y\right\|_L \le \left\|J\right\|_L \left\|\Delta u\right\|_L + \left\|J\right\|_L \left\|u_{k-1}\right\|_L . \quad (17)$$

From (14)-(17) we have,

$$\begin{aligned} \gamma_1 &= \left\|J^{-1}\right\|_L \cdot \left\|K\right\|_L \cdot \Delta t, \\ \gamma_2 &= \left\|J\right\|_L , \end{aligned} \quad (18)$$

$$\beta_1 = 0 \text{ and } \beta_2 = \left\|J \cdot u_{k-1}\right\| , \quad (19)$$

where $\beta_2 = J \cdot u_{k-1}$ is the bias term and considering a discrete system, it has a fixed value for each time step. This value depends on previous input, u_{k-1}. For the feedback connection to be finite gain L stable [21] as in (5),

$$\Delta t \cdot \left\|J^{-1}K\right\|_L \cdot \left\|J\right\|_L \le \Delta t \cdot \left\|J^{-1}\right\|_L \left\|K\right\|_L \left\|J\right\|_L < 1 , \quad (20)$$

must be true. A discrete time step $\Delta t = 1$ s is assumed since this gives the flow dynamics sufficient time to settle and it simplifies the controller design such that (20) becomes,

$$\left\|J^{-1}K\right\|_L \cdot \left\|J\right\|_L \le \left\|J^{-1}\right\|_L \left\|K\right\|_L \left\|J\right\|_L < 1 . \quad (21)$$

VI. Controller Evaluation

A. Methods and Procedures

Performance of the controller is evaluated in both FLUENT CFD simulations and in physical experiments using a 1:4 scale model of the TPAWT facility, Fig. 9. Evaluations determined the ability of the controller to regulate wind velocity at the user position. Feedback control (13) was used to control wind speed at the user by specifying bulk vent velocity (v_L+v_R). Feed-forward vent velocity ratios were then used to determine specific vent velocities and ultimately control wind angle at the user position.

The scale model incorporates actuated valves and a number of velocity sensors into our existing test-bed [22] in order to facilitate real-time flow control. The scale model is composed of a prime mover (Chicago axial blower with Toshiba ESP-130 frequency drive), a main plenum (1.22m x 1.22 m x 2.44 m settling chamber), butterfly throttling valves, ducting, inlet ducting, and a test section. Throttling valves are mounted on the side of the plenum and are actuated by geared (66:1) Maxon DC motors (20 W).

Ducting then connects the valves to the TPAWT test section. Round flexible ducts (3m long, 15.2 cm diameter) connect the valves to the inlet ducting, which includes honeycomb for flow conditioning. Inlet ducting transitions smoothly from round to square ducting (12.1 cm per side) and leads to a 56 cm long horizontal contraction. The contraction reduces from the aforementioned square cross section to a smaller rectangular cross section (6.0 cm by 12.1 cm) in order to accelerate the flow into the facility to reduce potential for backflow. Various duct lengths and configurations were

tested to ensure uniform flow into the TPAWT. The inlet vents are mounted symmetrically and form an angle Φ with the test section walls. The test section is comprised of Lexan (side walls, ceiling) and wood (floor) with dimensions indicated, Fig. 9. In order to approximate 2D flow, the aspect ratio was set to 1:9 by having the gap height between floor and ceiling be 13 cm throughout the test section.

The TPAWT test section is instrumented to facilitate active flow control. Pitot tubes at each of the inlet ducts measure differential pressures and determine vent velocities. Wind speed and direction at the user are determined by a custom pitot-vane sensor mounted at the user position. The vane was designed to orient the pitot tube along the streamlines of the flow. Dwyer 607-21 Differential Pressure Transmitters with a 250 ms response time were used to measure pitot tube pressures. Potentiometers measure valve angles and pitot-vane angle.

A dSpace 1103 Controller Board operating at a 1 kHz sampling rate is used to control the experimental apparatus from Simulink using the Real Time Workshop toolbox. The output feedback controller (13) provides commands to vent velocity controllers, which in turn provide commands to the throttle valve controllers. Traditionally designed PI controllers are used in all of these instances to minimize tracking error and reduce sensitivity to noise.

B. Simulations

FLUENT CFD simulations were used to evaluate the performance of (13). The system starts from rest (no initial wind velocity) and is given a desired 4.0 m/s wind speed at the user. Two desired wind directions that correlate to the stream functions shown in Fig. 4 (a) and (b) were evaluated ($v_L / v_R = 1.00$ for $\theta_{desired} = 0°$ and $v_L / v_R = 0.76$ for $45°$). The simulations were based upon quasi-steady flow and the time step was chosen to be $\Delta t = 1$ s in order to allow the flow dynamics to settle between control updates. At each time step, the flow field was simulated given the specified inlet vent velocities. The solution of each simulation was iterated until the convergence of pressure, velocity, and continuity within a residual tolerance of 10^{-5}. The wind velocity at the user was evaluated by averaging the wind speed and wind angle at the nodes along the line representing the user position shown in Fig. 4.

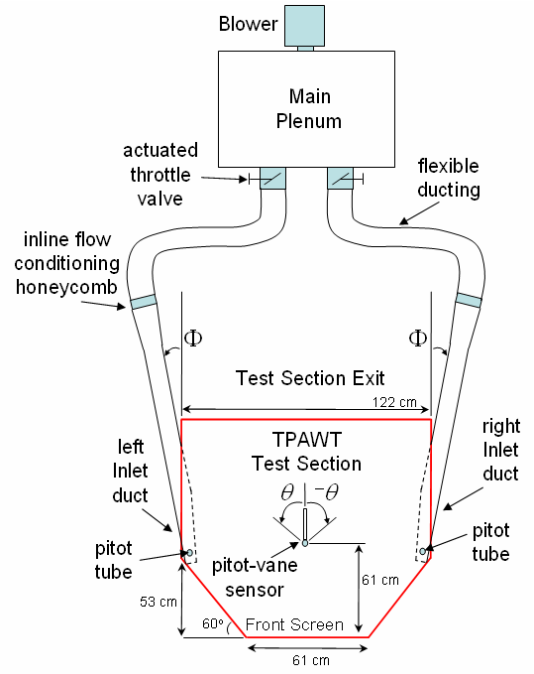

Fig. 9. Scale Model TPAWT facility.

The simulations for the case of $\theta_{desired} = 0°$ and $v_L / v_R = 1.00$ are shown in Fig. 10. The simulations also showed same accuracy and satisfactory results for $\theta_{desired} = 45°$,but are not shown here for the sake of brevity. In order to implement the controller, the specific Jacobian for this case was determined. Using a least squares estimate, it is found that the slope of the line in Fig. 6 is 1.03 with a zero intercept. Using this slope as the Jacobian in (13), a controlled input can be obtained. From (21), it can be inferred that a Jacobian, which is a scalar, in this case, gets cancelled, and the system will be stable as long as the gain K is less than unity for $\Delta t = 1$. Thus a gain of K = 0.9, which gives a slower settling time, is chosen. It can be seen from Fig 10(a), that the mean wind speed converges to the desired value of 4m/s in five iterations (seconds). Note that the range of wind speed along the line defining the user position varies between 3.0 and 4.5 m/s. As Fig. 10(b) indicates, the mean wind angle is exactly $0°$, but the angle of wind along the line varies from $-4.7°$ to $4.7°$.

C. Experiments

Experimental evaluations were conducted to evaluate the performance of controller (13) applied to the instrumented TPAWT scale model facility. Similar to simulations, a feed-forward vent velocity ratio ($v_L / v_R = 1$) was used to control wind angle at the user and (13) was used to provide feedback control of the wind speed. Unlike the simulations, though, it was not possible to start the controller with zero vent velocity due to leakage around the butterfly valves. Thus, these experiments evaluate the ability of the system to regulate wind speed at the user from 1 m/s to 4 m/s while ideally maintaining a wind heading of θ = 0˚.

Fig. 11 indicates the step response of the system. Note that the average velocity of the flow reaches the desired velocity within ~20 sec. Appreciable velocity fluctuations are apparent and are due to the turbulent nature of the wind and the dynamics of the vortices acting on the core flow. It is also worth noting that the angle of the wind varies between 10 and 15 degrees during this experiment, which was found to be typical. Tuning of the vent velocity ratio can reduce this error, but the ratio was left at unity to provide comparison to

the simulation results. Similar results are found for $\theta_{desired} = 45°$, but are not provided for brevity.

D. Discussion and Future Work

Simulations and experiments both demonstrate that the controller is capable of accurately regulating wind speed at the user position. As experimental results demonstrate, though, feed-forward vent velocity ratios alone are insufficient for accurately regulating wind angle.

These results represent significant improvement over previous findings that indicated that the core flow at the user was unstable [22]. In the absence of control, the previous results indicated that the core flow naturally bifurcated and approached stable equilibria at ±60°. The controller presented here maintains the flow at the user within 15˚of the desired value based upon feed forward vent velocity ratios and converges nominal wind speed within 0.2 m/s with a settling time of 20 s.

Angle accuracy can be improved by experimentally tuning the feed-forward term, applying additional feedback, or adding a negative pressure back plenum, which are all the subject of ongoing research. This point is supported by the results shown in Fig. 12, which demonstrate that basic PD control of wind angle (without wind speed control) is capable of reducing error from −20° to −6°. Improved control of settling time is also the subject of ongoing research. Issues include pitot tube sensor delays and resulting dynamics of vent velocity servo loops.

Ultimately, it is desired to regulate both wind angle and speed based upon output feedback control. One consideration is to derive 2x2 Jacobian for sensitivity of speed and angle given vent velocity variations. The resulting control law derivation could then be extended to this application, but the Jacobian would not drop out as in this paper. The theoretical basis for the controller shown in Section V is actually intended to solve the 3D wind control problem. While the Jacobian portion of the Small Gain Theorem proved to be simple in the case of the single-input-single-output controller, this is not expected to be the case with controlled heading and velocity.

While wind speed and velocity do vary at the user position, these results are expected to be suitable for haptic display, which is the subject of this ongoing research. Future work will focus on improving accuracy for using the TPAWT system for other scientific applications. We will also focus on creating more complex flow patterns with faster dynamics

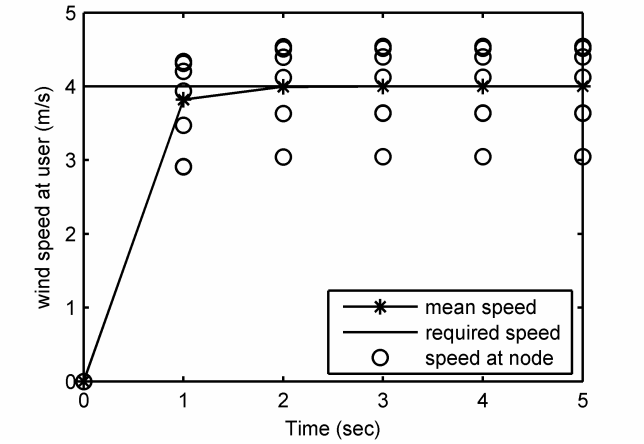

(a) Wind Speed at User

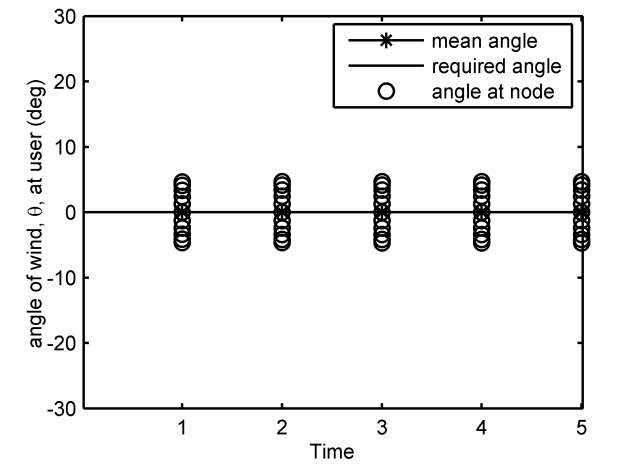

(b) Wind Angle at User

Fig. 10. Controller simulation for $\theta_{desired} = 0°$, $v_L / v_R = 1.00$.

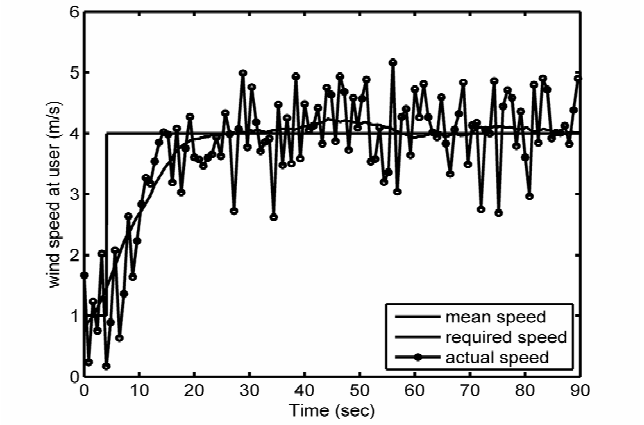

(a) Wind Speed at User

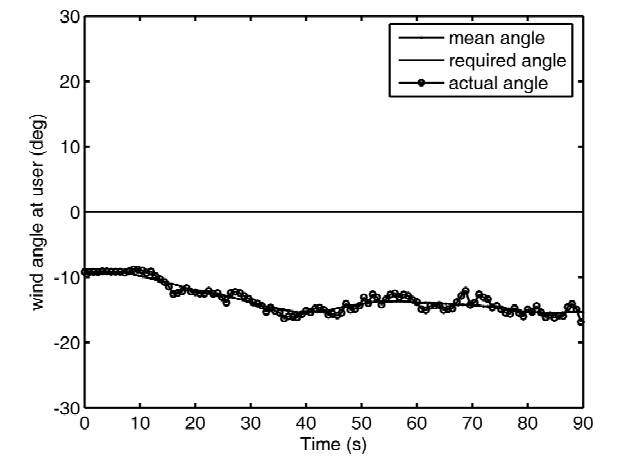

(b) Wind Angle at User

Fig. 11. Experiments for $\theta_{desired} = 0°$ and $v_L / v_R = 1.00$.

such as gusts, crosswinds, and shear flows.

The current controller design is well suited to real-time active control of this system since the computational load of (13) is minimal. Comparatively, the CFD simulations required ~60 s per time step on a 2.4 GHz dual processor Sun Fire V490 machine whereas the proposed controller required <1 ms per step on a 400 MHz dSpace 1103 Controller. Considering the CFD model to predict the control actions rather than our method, the CFD model would require 5.4×10^6 seconds to predict the experimental control actions. Model reduction techniques such as POD and AIM offer reduction of this time requirement, which is a subject of future work.

Transitioning to the full scale Treadport system is also underway. Issues include packaging equipment within available lab space, conditioning air flow under non-ideal conditions, incorporating non-intrusive sensors, and extending these controller results to three dimensional space.

VII. Conclusion

A method of real-time flow control for the Treadport Active Wind Tunnel (TPAWT) is presented. It is based upon creating stable flow patterns that result from counter rotating vortices. The control law is based upon the small gain theorem, output feedback, and a dynamic extension. The feedback controller for speed and the feed-forward angle controller provide reasonably accurate control of wind at the user's position. CFD simulations and experimental validations confirm these results.

Acknowledgment

The authors would like to thank Charles Fisher, John Hollerbach, Meredith Metzger, Pete Willemsen, Richard Kirkman, David Grow, Dustin Wallis, Akshay Gowardhan, Hamid Sani and Paulo Botero for their inspiration and collaboration in this ongoing project.

References

[1] J. Hollerbach, D. Grow, and C. Parker, "Developments in locomotion interfaces," *2005 IEEE 9th International Conference on Rehabilitation Robotics, 28 June-1 July 2005*, 2005, Chicago, IL, pp. 522-5, 2005.

[2] D. I. Grow and J. M. Hollerbach, "Harness design and coupling stiffness for two-axis torso haptics," *14th Symp. Haptic Interfaces for Virtual Environments and Teleoperator Systems*, March 25-26, Arlington, VA, pp.14, 2006.

[3] M. Metzger, R. Kirkman, "Conceptual Design of an adaptive wind tunnel for the generation of an unsteady complex flow patterns," *ASME 2005 Fluids Engineering Division Summer Meeting and Exhibition*, Houston, Texas, June 19-23, pp. 169-178, 2005.

[4] D. Dochain, J. P. Babary, and N. Tali-Maamar, "Modelling and adaptive control of nonlinear distributed parameter bioreactors via orthogonal collocation," *Automatica*, vol. 28, pp. 873-883, 1992.

[5] A. A. Patwardhan, G. T. Wright, and T. E. Edgar, "Nonlinear model-predictive control of distributed-parameter systems," *Chemical Engineering Science*, vol. 47, pp. 721-735, 1992.

[6] P. K. Gundepudi and J. C. Friedly, "Velocity control of hyperbolic partial differential equation systems with single characteristic variable," *Chemical Engineering Science*, vol. 53, pp. 4055-4072, 1998.

[7] W.H.Ray, *Advanced Process Control*. New York: McGraw Hill, 1981.

[8] H. Choi, R. Temam, P. Moin, and J. Kim, "Feedback control for unsteady flow and its application to the stochastic Burgers equation," *Journal of Fluid Mechanics*, vol. 253, pp. 509-43, 1993.

[9] S. S. Joshi, J. L. Speyer, and J. Kim, "A systems theory approach to the feedback stabilization of infinitesimal and finite-amplitude disturbances in plane Poiseuille flow," *Journal of Fluid Mechanics*, vol. 332, pp. 157-84, 1997.

[10] M. Desai and K. Ito, "Optimal controls of Navier-Stokes equations," *SIAM Journal on Control and Optimization*, vol. 32, pp. 1428-1446, 1994.

[11] T. R. Bewley, R. Temam, and M. Ziane, "A general framework for robust control in fluid mechanics," *Physica D*, vol. 138, pp. 360-92, 2000.

[12] A. A. Panagiotis D.Christofides, "Nonlinear Control of Navier Stokes Equations," *Proceedings of the American Control Conference*, Philadelphia, PA, pp1355-9, 1998.

[13] B. B. King and Y.-R. Ou, "Nonlinear dynamic compensator design for flow control in a driven cavity," *Proceedings of the 1995 34th IEEE Conference on Decision and Control. Part 4 (of 4), Dec 13-15 1995*, New Orleans, LA, USA, pp. 3741-3746, 1995.

[14] S. S. Ravindran, "A reduced-order approach for optimal control of fluids using proper orthogonal decomposition," *International Journal for Numerical Methods in Fluids*, vol. 34, pp. 425-48, 2000.

[15] A. Chatterjee, "An introduction to the proper orthogonal decomposition," *Current Science*, vol. 78, pp. 808-17, 2000.

[16] A. Armaou and P. D. Christofides, "Dynamic Optimization of Dissipative PDE Systems Using Nonlinear Order Reduction" *Proceedings of the 41st IEEE Conference on Decision and Control, Dec 2002*, Las Vegas, Nevada, USA, pp. 5083-5114, 2002.

[17] E. H. Dowell, K. C. Hall, and M. C. Romanowski, "Eigenmode analysis in unsteady aerodynamics: reduced order models," *Applied Mechanics Reviews*, vol. 50, pp. 371-385, 1997.

[18] J. A. Burns and D. Rubio, "Distributed parameter control approach to sensor location for optimal feedback control of thermal processes," *Proceedings of the 1997 36th IEEE Conference on Decision and Control. Part 3 (of 5), Dec 10-12 1997*, San Diego, CA, USA, pp. 2243-2247, 1997.

[19] R. S. Chandra and R. D'Andrea, "Necessity of the small gain theorem for multidimensional systems," *Proc. 42nd IEEE Conference on Decision and Control, Dec 9-12 2003*, Maui, HI, United States, pp. 2859-2864, 2003.

[20] R. D'Andrea and G. E. Dullerud, "Distributed Control Design for Spatially Interconnected Systems," *IEEE Transactions on Automatic Control*, vol. 48, pp. 1478-1495, 2003.

[21] H. K. Khalil, *Nonlinear Systems*, Third Edition ed, 1996.

[22] R. Kirkman, M. Deaver, E. Pardyjak, and M. Metzger, "Sensitivity Analysis of a Three-Dimensional Wind Tunnel Design," *2006 ASME Joint U.S.-European Fluids Engineering Summer Meeting, FEDSM 2006,* July 17-20, Miami, FL, pp. 10, 2006.

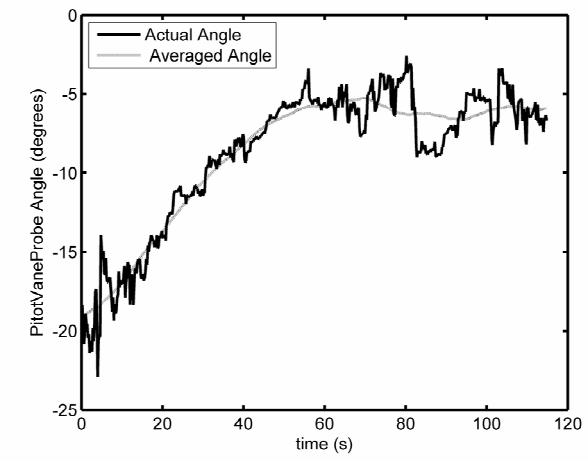

Fig. 12. Experimental angle tracking and stabilization for output angle feedback controller.